Effect of Strains on the Dark Current-Voltage Characteristic of Silicon Heterojunction Solar Cells

Laurent Guin, Pere Roca I Cabarrocas, Michel E Jabbour, Nicolas Triantafyllidis

Effect of strain on the dark current-voltage characteristic of silicon heterojunction solar cells

L. Guin[a,b,1], P. Roca i Cabarrocas[b,*], M. E. Jabbour[a,c], N. Triantafyllidis[a,c,d]

[a]*LMS, École polytechnique, CNRS, Institut polytechnique de Paris, 91128 Palaiseau, France*
[b]*LPICM, École polytechnique, CNRS, Institut polytechnique de Paris, 91128 Palaiseau, France*
[c]*Département de Mécanique, École polytechnique, 91128 Palaiseau, France*
[d]*Aerospace Engineering Department & Mechanical Engineering Department (emeritus), The University of Michigan, Ann Arbor, MI 48109-2140, USA*

Abstract

Anisotropic mechanical strain as low as 0.1% modifies the electronic response of crystalline semiconductor-based devices and in particular affect the performance of solar cells. We measure the dark current-voltage characteristic of silicon heterojunction solar cells under different levels of tensile uniaxial stress and observe a reversible change of the *j-V* curve with applied strain. Using a two-exponential description of the *j-V* characteristic to fit our experimental data, we obtain the strain dependence of the diffusion saturation current and find a decrease of about 3% for a tensile strain level of 6.7×10^{-4}. We compare these experiments to a theoretical model that accounts for the effect of strain on the band energy levels, densities of states and mobilities of carriers. The theoretical estimation of the change in saturation current is found to be in reasonable agreement with experimental results.

Keywords: strain effect, stress, mechanical loading, solar cell, piezojunction effect.

1. Introduction

Mechanical anisotropic strain, by breaking the symmetry of the atomic lattice, modifies the electronic properties of crystalline semiconductors. In crystalline silicon, the

*Corresponding author.
Email address: pere.roca@polytechnique.edu (P. Roca i Cabarrocas)
[1]Present address: Mechanics & Materials, Department of Mechanical and Process Engineering, ETH Zürich, Zürich 8092, Switzerland.

strain dependence of these electronic properties has been investigated both theoretically for the band energy levels and densities of states of the conduction and valence bands by through deformation potential theory (Bardeen and Shockley, 1950; Herring and Vogt, 1956; Bir et al., 1974; Fischetti and Laux, 1996; Creemer, 2002) and experimentally for the mobilities of carriers (Smith, 1954; Kanda, 1991; Kleimann et al., 1998; Lange et al., 2016). At the macroscale, strain modifies the electronic response of electronic devices such as *p-n* junctions (Wortman et al., 1964; Wortman and Hauser, 1966; Kanda, 1967; Rueda, 1999) and transistors (Creemer and French, 2000; Creemer et al., 2001; Creemer, 2002), a phenomenon called the *piezojunction effect*. In the early experimental studies of this effect on *p-n* junctions (Imai et al., 1965; Rindner, 1965; Wooten et al., 1968), strains were applied through an indenter tip or by bonding the device to a substrate subjected to deformations, which introduced complex strain spatial distributions and uncertainties in the strain field that develops in the device. While for the high level of stress ($\sim 1\,\mathrm{GPa}$) exerted in these experiments, the predominant mechanism in the piezojunction effect is the change in band energy levels (Wortman et al., 1964; Wortman and Hauser, 1966; Kanda, 1967), more sophisticated models are necessary for lower levels of stress, as typically encountered in real applications. Indeed, for moderate stress levels in transistors ($\sim 100\,\mathrm{MPa}$), Creemer and French (2000) pointed out that the strain dependences of the band energy levels, densities of states, and mobilities have comparable contributions to the piezojunction effect.

Solar cells are a large domain of applications of *p-n* junctions, where stresses may be encountered both during the fabrication process and in device use, in particular with emerging flexible solar cells (Pagliaro et al., 2008; Velut et al., 2014). Existing works on the effect of stress on the performance of solar cells concern amorphous silicon solar cells and are limited to experimental investigations (Jones et al., 2002; Gleskova et al., 2006; Chen et al., 2018; Dai et al., 2019). Indeed, because the strain-dependence of the electronic properties of amorphous materials is currently not well known, the modeling of the effect of stress on the electronic response of devices based on these materials remains difficult. By contrast, with crystalline-based solar cells, one may use the extensive knowledge on the strain-dependence of the properties of crystalline silicon to develop an understanding of the mechanisms underlying the effect

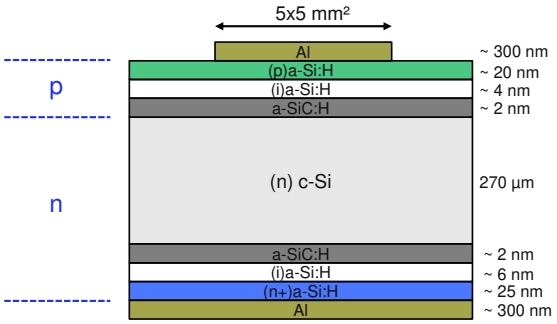

Figure 1: Structure of the silicon heterojunction solar cell.

of strain on their electronic response. This is what we propose in the present work by investigating both experimentally and through modeling the strain-induced changes in the electronic reponse of silicon heterojunction solar cells.

The rest of the article is organized as follows. In Section 2, we present the experimental pocedure consisting of the fabrication of Silicon HeteroJunction (SHJ) solar cells and the setup used for the combined electro-mechanical measurements. Experimental results on the strain dependence of the *j-V* curve under uniaxial tension are given in Section 3, whereas a theoretical model for this effect is proposed in Section 4. Finally, we draw concluding remarks in Section 5.

2. Experimental

2.1. Silicon heterojunction solar cells

The SHJ solar cells used in the experiments are fabricated from a commercial (100) n-doped c-Si wafer of resistivity 2.6 Ω.cm. After dipping the wafer for 30 s in a solution of 5% HF, a-SiC:H and a:Si-H layers are deposited in a Plasma-Enhanced Chemical Vapor Deposition (PECVD) at 175°C. Aluminum electrodes are subsequently deposited by thermal evaporation in vacuum and the resulting cells are annealed at 180°C for 15 min to improve the carrier lifetime. The resulting structure of the solar cell is shown on Fig. 1. Note that, for the evaporation of the top electrode, we use a mask with square cell sections of $5 \times 5\,\mathrm{mm}^2$ with sides oriented along the $\langle 110 \rangle$ directions. After fabri-

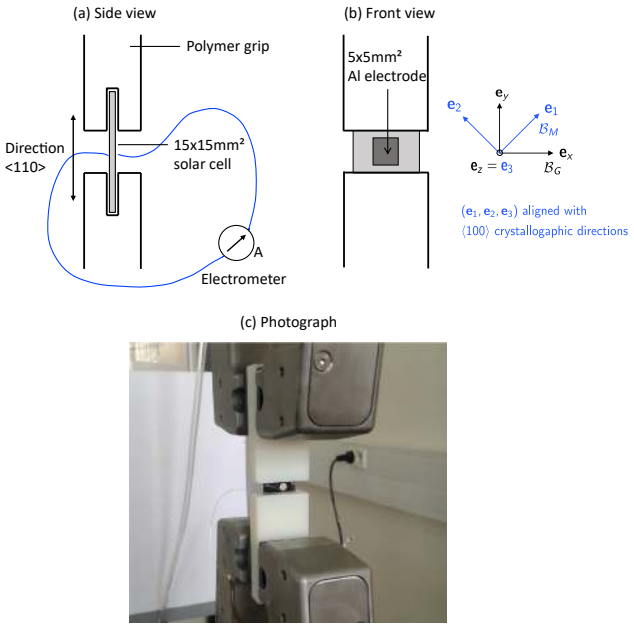

Figure 2: Schematic [(a) and (b)] and photograph (c) of the experimental set-up, with the 15×15 mm^2 solar cell glued inside the grooves of polymer grips. $\mathscr{B}_M = (\mathbf{e}_1, \mathbf{e}_2, \mathbf{e}_2)$ (M for material) is an orthonormal basis aligned with the $\langle 100 \rangle$ directions of the crystal; $\mathscr{B}_G = (\mathbf{e}_x, \mathbf{e}_y, \mathbf{e}_z)$ (G for grips) is obtained by rotating $\mathscr{B}_M$ by $\pi/4$ in the clockwise direction and has its vector $\mathbf{e}_y$ aligned with the loading direction.

cation, the cells are separated by cutting $15 \times 15\,\text{mm}^2$ squares providing space around each cell for gripping it throughout the mechanical loading.

2.2. *Setup for mechanical loading*

To load mechanically the solar cells, we use an Instron 3366 electromechanical testing machine with home-made three-dimensional printed grips. As depicted in Fig. 2, the 15×15 mm^2 and $270\,\mu$m thick solar cell is glued inside the $500\,\mu$m grooves of the polymer grips. Note that the sample is glued after the grips have been set in the testing machine in order to avoid exerting pre-stress on the silicon wafer.

In such a configuration, the silicon sample carries all the uniaxial load exerted by the testing machine. Moreover, given that the stiffness of the polymer grips (Young's modulus is about 2.4 GPa) is much smaller than that of silicon (elastic coefficients of

the order of 100 GPa), we can assume the silicon wafer to be in a state of uniaxial stress. Using the elastic properties of silicon (described by the elasticity tensor $\mathbf{c}$ of silicon Wortman and Evans, 1965), we can derive its strain state (described by the small strain tensor $\boldsymbol{\varepsilon}$) from the load F measured by the load cell of the testing machine with

$$\boldsymbol{\varepsilon} = \mathbf{c}^{-1} : \boldsymbol{\sigma}, \tag{1}$$

where the stress state $\boldsymbol{\sigma}$ is approximately given by

$$\boldsymbol{\sigma} = \frac{F}{S}\mathbf{e}_y \otimes \mathbf{e}_y, \tag{2}$$

with $\mathbf{e}_y$ the loading direction (cf. Fig. 2) and S the section area of the silicon sample in the $(\mathbf{e}_x, \mathbf{e}_z)$ plane.

2.3. Electrical measurements

For the electrical measurements, the solar cell is connected to a Keithley 2460 sourcemeter using gold wires bonded with silver paste to its front and back electrodes. With this set-up, the current-voltage characteristic of the solar cell is measured for different loading forces: $F = 200\,\mathrm{N}$ ($\varepsilon_{yy} = 2.7 \times 10^{-4}$), $F = 300\,\mathrm{N}$ ($\varepsilon_{yy} = 4.1 \times 10^{-4}$), $F = 400\,\mathrm{N}$ ($\varepsilon_{yy} = 5.4 \times 10^{-4}$), and $F = 500\,\mathrm{N}$ ($\varepsilon_{yy} = 6.8 \times 10^{-4}$), which is the last level of loading before the failure of the sample. At the different load levels, the displacement of the grips is maintained fixed for about one minute, which is the time needed to measure the *j-V* characteristic. Note that, in order to check the reversibility with deformation of the change in the characteristic, we return to zero load ($F = 0$) between the different loading levels and measure, in these relaxed states, the *j-V* characteristics.

3. Results

3.1. Dark current-voltage characteristics under mechanical loading

Fig. 3 shows the current-voltage characteristic of a particular solar cell for different levels of applied strain. At the scale of Fig. 3 (a), the *j-V* curves superimpose and the effect of strain is not visible; we therefore plot them in Fig. 3 (b) in the restricted voltage range $0.381\,\mathrm{V} - 0.383\,\mathrm{V}$. Curves 1 and 2 at zero-strain are two measurements

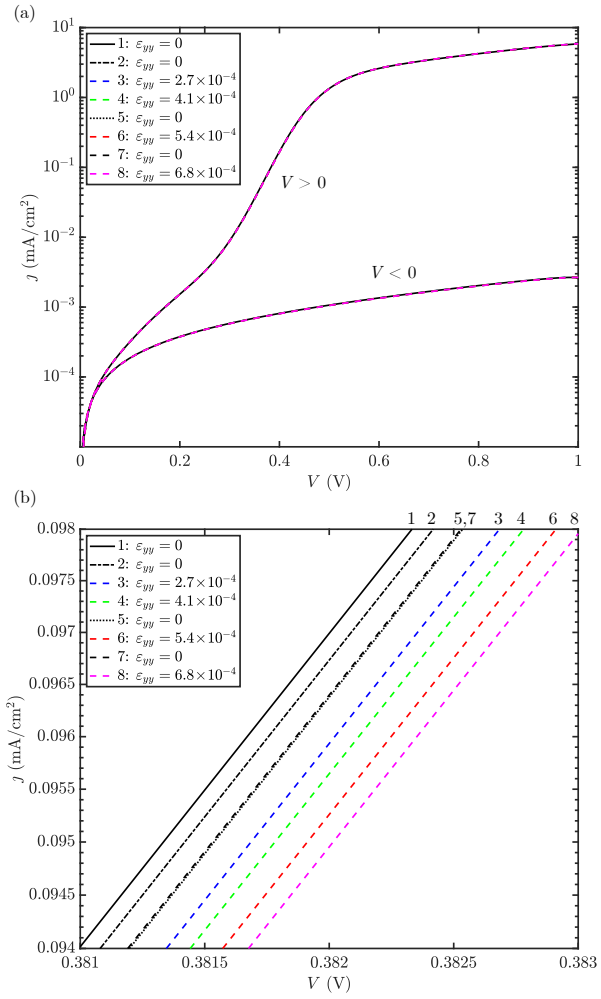

Figure 3: Current-voltage characteristics of a SHJ solar cell under different levels of applied strain. In (a) the voltage ranges from $-1\,\mathrm{V}$ to $1\,\mathrm{V}$, whereas (b) is a zoom on the range $0.381\,\mathrm{V} - 0.383\,\mathrm{V}$. Numbers 1 to 8 indicate the chronological order of mechanical loadings and unloadings.

performed with an interval of 12 h, the drying time for the glue. Curves 3 and 4 display a shift in characteristic induced by the first two strain levels and Curve 5 at zero-strain shows a small residual irreversible part in the mechanically-induced change. Moreover, whereas changes with further increments of strain are displayed by Curves 6 and 8, one can see on Curve 7 at zero-strain that the residual change observed in step 5 has not been increased. Hence, while the first level of loading may have induced some irreversible change in the cell, most of the contribution to the strain-induced change is indeed due to elastic deformation of the semiconductor.

Note that our experimental results agree well with those performed by Rueda (1999) on purely crystalline silicon *p-n* junctions in the context of integrated circuit. In this work, the authors used a four-point bending flexural test to measure the effect of both compressive and tensile stress on the *j-V* characteristic of planar and lateral *p-n* junctions. Notwithstanding the difference with our experimental set-up, in that the four-point bending induces a non-uniform strain field, their measurements of the decrease in the direct current under tensile strain are comparable to ours.

3.2. Strain dependence of the diffusion saturation current

In order to quantify the strain dependence of the parameters of the cell, in particular of the diffusion saturation current $j_s(\varepsilon)$, we use a two-exponential model (Wolf et al., 1977; Suckow et al., 2012) of the *j-V* relation with effective series resistance $R_s(\varepsilon)$ and parallel resistance $R_p(\varepsilon)$ to fit the experimental data:

$$j = \underbrace{j_s(\varepsilon)\left(\exp\left(\frac{q\big(V-jR_s(\varepsilon)\big)}{k_BT}\right)-1\right)}_{\text{Diffusion current}} + \underbrace{j_r(\varepsilon)\left(\exp\left(\frac{q\big(V-jR_s(\varepsilon)\big)}{2k_BT}\right)-1\right)}_{\text{Recombination-generation current}} + \underbrace{\frac{V-jR_s(\varepsilon)}{R_p(\varepsilon)}}_{\text{Parallel resistance current}}, \tag{3}$$

with $j_r(\varepsilon)$ the saturation current of the Recombination-Generation (RG) current (Sze and Ng, 2006), q the elementary charge, k_B the Boltzmann constant and T the abso-

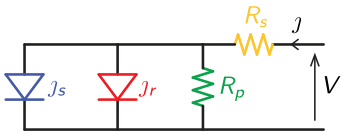

Figure 4: Equivalent electric circuit for the two-exponential model with j-V expression (3).

Table 1: Best fit parameters of (3) with the experimental j-V characteristic of the solar cell of Fig. 3 for a fit over the range $(-1\,\mathrm{V}, 1\,\mathrm{V})$.

j_s	j_r	R_s	R_p
$(\mathrm{mA/cm^2})$	$(\mathrm{mA/cm^2})$	$(\Omega\cdot\mathrm{cm^2})$	$(\Omega\cdot\mathrm{cm^2})$
3.7×10^{-8}	1.5×10^{-5}	71	4.9×10^{5}

lute temperature. The equivalent electric circuit corresponding to the two-exponential model (3) is shown on Fig. 4.

Note that, in contrast with j_s, we do not have physical models for the dependence of j_r, R_s, and R_p on strain. Indeed, R_s and R_p are phenomenological quantities introduced to account for the parasitic resistances of various physical origins (e. g., contact resistance, resistance of the semiconductor layers, shunts). Likewise, since j_r is associated with recombination in the space charge region, it involves electronic properties of both the crystalline and amorphous silicon, the strain dependence of the latter being unknown.

To determine the four model parameters j_s, j_r, R_s and R_p from the experimental j-V characteristics, we use the algorithm developed by Suckow et al. (2012) (see also Suckow, 2014) based on a least-square fit of Eq. (3) to the experimental data. The parameters obtained from the j-V curve of Fig. 3 are summarized in Table 1. Then the strain dependence of the cell parameters is obtained by carrying out, at the different loading steps, two different fitting procedures as follows:

1. *Fit 1*: In the first procedure, the fit is performed over the range $(-1\,\mathrm{V}, 1\,\mathrm{V})$ with respect to the four parameters j_s, j_r, R_s and R_p, for all the loading levels.
2. *Fit 2*: For comparison, we use a second fitting procedure restricted to the range $(0.2\,\mathrm{V}, 0.5\,\mathrm{V})$ with R_s and R_p kept fixed across the fits at different loading levels. Indeed, since in this range j_s contributes predominantly to the total current, it

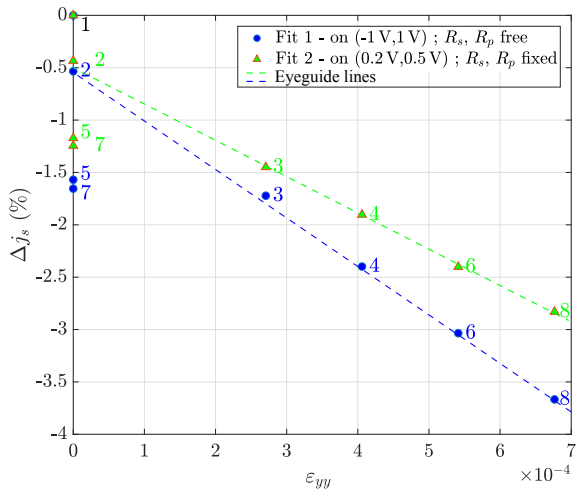

Figure 5: Relative change $\Delta j_s := (j_s(\boldsymbol{\varepsilon}) - j_s(\mathbf{0}))/j_s(\mathbf{0})$ of the diffusion saturation current associated with the *j-V* curves of Fig. 3 with the two fitting procedures Fit 1 and Fit 2.

corresponds to the region where there is most of the information on it.

The relative changes in j_s, as defined by $\Delta j_s(\boldsymbol{\varepsilon}) := (j_s(\boldsymbol{\varepsilon}) - j_s(\mathbf{0}))/j_s(\mathbf{0})$, are reported on Fig. 5. One can see a relative change in the diffusion saturation current of about -3% for a strain of $\sim 7 \times 10^{-4}$. The difference between the two methods gives an idea of the uncertainty on that measurement, which is about 1% in absolute value.

4. Modeling of the strain-effect

To interpret the measurements of the strain-induced change in the diffusion saturation current, we use a model accounting for the strain dependence of the following electronic properties of silicon: band energy levels ($E_c(\boldsymbol{\varepsilon})$ and $E_v(\boldsymbol{\varepsilon})$) and densities of states ($N_c(\boldsymbol{\varepsilon})$ and $N_v(\boldsymbol{\varepsilon})$) of the conduction and valence bands, as well as mobilities ($m_n(\boldsymbol{\varepsilon})$ and $m_p(\boldsymbol{\varepsilon})$) of electrons and holes (Guin et al., 2018; Guin, 2018). We model the solar cell as a *p-n* heterojunction with *p*- and *n*-doped regions—corresponding to the (p)a-Si:H layer and (n)c-Si wafer, cf. Fig. 1—with thicknesses W_p and W_n, respectively. Note that the intrinsic amorphous silicon, *n*-doped amorphous silicon, and silicon carbide layers that are part of the solar cell structure shown on Fig. 1 are buffer and passi-

vation layers which are not explicitly modeled. However, the influence of these layers on the electric response appears through the effective surface recombination velocities S_n on the front side (top of (p)a-Si:H layer) and S_p on the back side (bottom of (n)c-Si layer). Let τ_n and τ_p be the carrier lifetimes and denote by $L_n(\varepsilon) := \sqrt{U_T m_n(\varepsilon)\tau_n}$ and $L_p(\varepsilon) := \sqrt{U_T m_p(\varepsilon)\tau_p}$ the associated diffusion lengths where $U_T := k_B T/q$ is the thermal voltage. Note that our focus being on the strain-induced changes in the current, only relative changes in currents and not their absolute values are relevant. As a result, as long as surface recombination velocities and carrier lifetimes are supposed independent of strain, their values are not needed. The expression of the diffusion saturation current is a generalization of the Shockley relation (Nelson, 2003; Fonash, 2012):

$$j_s = j_{sn} + j_{sp}, \tag{4}$$

where j_{sn} and j_{sp} are the contributions to the diffusion saturation current of the layers (p)a-Si:H and (n)c-Si, respectively, with expressions:

$$\begin{aligned} j_{sn} &= q(n_i^a)^2 \frac{U_T m_n}{N_a L_n} \frac{\frac{L_n S_n}{U_T m_n}\cosh(W_p/L_n) + \sinh(W_p/L_n)}{\frac{L_n S_n}{U_T m_n}\sinh(W_p/L_n) + \cosh(W_p/L_n)}, \\ j_{sp} &= q(n_i^c)^2 \frac{U_T m_p}{N_d L_p} \frac{\frac{L_p S_p}{U_T m_p}\cosh(W_n/L_p) + \sinh(W_n/L_p)}{\frac{L_p S_p}{U_T m_p}\sinh(W_n/L_p) + \cosh(W_n/L_p)}, \end{aligned} \tag{5}$$

where N_a and N_d are the acceptor and donor dopant concentrations, and $n_i^a(\varepsilon)$ and $n_i^c(\varepsilon)$ are the intrinsic carrier concentrations in the (p)a-Si:H layer and (n)c-Si wafer, respectively. The latter involve the density of states and band gap $E_{gap}(\varepsilon) := E_c(\varepsilon) - E_v(\varepsilon)$ for amorphous and crystalline silicon according to:

$$\begin{aligned} (n_i^a)^2 &= N_c^a N_v^a \exp\big[-E_{gap}^a/k_B T\big], \\ (n_i^c)^2 &= N_c^c N_v^c \exp\big[-E_{gap}^c/k_B T\big], \end{aligned} \tag{6}$$

where the superscripts a and c are associated to the amorphous and crystalline layers, respectively. Given the state of homogeneous strain to which the cell is subjected, the change with strain of j_s can be directly computed from Eqs. (4)-(5) using the strain dependence of the band energy levels, densities of states and carrier mobilities.

Experiments measuring the temperature dependence of j_s in SHJ solar cells similar to ours (Taguchi et al., 2008) yield an exponential dependence with $-1/T$ with an

activation energy of 1.13 eV. This value, which corresponds to the band gap of crystalline silicon, indicates that the component j_{sp} coming from the crystalline wafer is predominant in Eq. (4), that is,

$$j_s(\varepsilon) \approx j_{sp}(\varepsilon). \tag{7}$$

It turns out that for the particular crystallographic directions chosen in the experiments (uniaxial stress along direction $\langle 110 \rangle$ and current and voltage along direction $\langle 100 \rangle$ as shown on Fig. 2), the strain dependence in the hole mobility can be neglected (see details in the Supplementary Material). Moreover, N_c in silicon has also a negligible dependence on strain (Kanda, 1967; Bir et al., 1974; Kleimann et al., 1998; Creemer, 2002). As a result, the saturation current simplifies to

$$\begin{aligned} j_s(\varepsilon) \;=\; & qN_c^c(\varepsilon)N_v^c \exp\left[\left(E_v^c(\varepsilon) - E_v^c(\varepsilon)\right)/k_BT\right] \times \\ & \frac{U_T m_p}{N_d L_p} \frac{\frac{L_p S_p}{U_T m_p}\cosh\left(W_n/L_p\right) + \sinh\left(W_n/L_p\right)}{\frac{L_p S_p}{U_T m_p}\sinh\left(W_n/L_p\right) + \cosh\left(W_n/L_p\right)}, \end{aligned} \tag{8}$$

where, in Eq. (8), the significant dependence of the electronic parameters on ε have been explicitly written. In turn, the relative change in saturation current with strain can be linearized as

$$\Delta j_s(\varepsilon) := \frac{j_s(\varepsilon) - j_s(\mathbf{0})}{j_s(\mathbf{0})} = -\frac{\Delta E_c^c(\varepsilon)}{k_BT} + \frac{\Delta E_v^c(\varepsilon)}{k_BT} + \frac{\Delta N_v^c(\varepsilon)}{N_v^c(\mathbf{0})}. \tag{9}$$

Numerically, with the strain state of the experiment given by Eq. (1), we obtain for $\varepsilon_{yy} = 6.8 \times 10^{-4}$ (cf. the Supplementary Material for the expressions of the strain-dependent electronic parameters $E_c^c(\varepsilon)$, $E_v^c(\varepsilon)$ and $N_v^c(\varepsilon)$),

$$\Delta j_s = \underbrace{-7\%}_{-\frac{\Delta E_c^c}{k_BT}} \underbrace{+7\%}_{\frac{\Delta E_v^c}{k_BT}} \underbrace{-6\%}_{\frac{\Delta N_v^c}{N_v^c}} = -6\%. \tag{10}$$

The change in saturation current of -6% predicted by the theory is about twice what we have measured. From the decomposition Eq. (10), we can see that the predicted variation of -6% results from the combination of the positive and negative effects of the various parameters, among which the effect of strain on the density of states of the valence band. It is likely that the discrepancy between the experimental result and

the modeling essentially comes from the limited knowledge of the strain dependence $N_v(\varepsilon)$. Indeed, while this parameter has a significant contribution to the total change in saturation current, the dependence of N_v on the triaxiality of the small strain tensor ε is still not well known (cf. the discussion on $N_v(\varepsilon)$ in the Supplementary Material).

5. Conclusion

In conclusion we have devised an experimental set-up that allows to measure the effect of uniform strain on the dark current-voltage characteristic of a solar cell. We observe a reversible effect and use a two-exponential description to obtain the strain-induced change in the diffusion saturation current, which shows a decrease of the order of 3% for a strain with a longitudinal component of 6.8×10^{-4}. We compare this value with that predicted by a model of the *p*-*n* heterojunction that accounts for strain-dependent carrier mobilities, band energy levels and densities of states. Specifically, the model predicts, for the strain state encountered in the experiment, a decrease in the diffusion saturation current of about 6%. This prediction is in agreement with experiments within a factor of two, a discrepancy that can be accounted for by the incomplete knowledge of the effect of strain on the density of states of the valence band.

Finally, note that in this work, we have investigated the strain effect on SHJ solar cells, a technology with relatively thick silicon ($270\,\mu$m), which limits the maximum reachable strain at typically 1×10^{-3}. At these levels of strain, the change in the current-voltage characteristic is measurable but small (a few percent), suggesting that the behavior of the cell is not strongly affected by strain. By contrast, the strain effect could be significantly larger with the higher levels of strain that may be reached in thinner crystalline solar cell technologies (Bergmann, 1999; Chopra et al., 2004), thus motivating further investigations.

Supplementary material

Supplementary Material for this article can be found online.

Acknowledgments

L. Guin thanks W. Chen for his help for the fabrication of the solar cells and V. De Greef for suggesting the loading set-up. This work was supported by the "IDI 2015" project funded by the IDEX Paris-Saclay, ANR-11-IDEX-0003-02.

References

Bardeen, J., Shockley, W., 1950. Deformation potentials and mobilities in non-polar crystals. Physical Review 80, 72–80. doi:10.1103/physrev.80.72.

Bergmann, R., 1999. Crystalline si thin-film solar cells: a review. Applied Physics A: Materials Science & Processing 69, 187–194. doi:10.1007/s003390050989.

Bir, G.L., Pikus, G.E., Shelnitz, P., Louvish, D., 1974. Symmetry and strain-induced effects in semiconductors. volume 624. Wiley New York.

Chen, A., Yossef, M., Zhang, C., 2018. Strain effect on the performance of amorphous silicon and perovskite solar cells. Solar Energy 163, 243–250. doi:10.1016/j.solener.2018.01.057.

Chopra, K.L., Paulson, P.D., Dutta, V., 2004. Thin-film solar cells: an overview. Progress in Photovoltaics: Research and Applications 12, 69–92. doi:10.1002/pip.541.

Creemer, J., French, P., 2000. The piezojunction effect in bipolar transistors at moderate stress levels: a theoretical and experimental study. Sensors and Actuators A: Physical 82, 181 – 185. doi:10.1016/S0924-4247(99)00362-3.

Creemer, J.F., 2002. The effect of mechanical stress on bipolar transistor characteristics. Ph.D. thesis. Delft University of Technology. URL: http://resolver.tudelft.nl/uuid:ff17cb76-7599-486b-b287-3123c806ac0f.

Creemer, J.F., Fruett, F., Meijer, G.C.M., French, P.J., 2001. The piezojunction effect in silicon sensors and circuits and its relation to piezoresistance. IEEE Sensors Journal 1, 98–. doi:10.1109/JSEN.2001.936927.

Dai, Y., Huang, Y., He, X., Hui, D., Bai, Y., 2019. Continuous performance assessment of thin-film flexible photovoltaic cells under mechanical loading for building integration. Solar Energy 183, 96–104. doi:10.1016/j.solener.2019.03.018.

Fischetti, M.V., Laux, S.E., 1996. Band structure, deformation potentials, and carrier mobility in strained si, ge, and SiGe alloys. Journal of Applied Physics 80, 2234. doi:10.1063/1.363052.

Fonash, S., 2012. Solar cell device physics. Elsevier. doi:10.1016/C2009-0-19749-0.

Gleskova, H., Cheng, I.C., Wagner, S., Sturm, J.C., Suo, Z., 2006. Mechanics of thin-film transistors and solar cells on flexible substrates. Solar Energy 80, 687–693. doi:10.1016/j.solener.2005.10.010.

Guin, L., 2018. Electromechanical couplings and growth instabilities in semiconductors. Ph.D. thesis. Université Paris-Saclay - Ecole polytechnique. URL: https://tel.archives-ouvertes.fr/tel-02124459.

Guin, L., Jabbour, M., Triantafyllidis, N., 2018. The p-n junction under nonuniform strains: general theory and application to photovoltaics. Journal of the Mechanics and Physics of Solids 110, 54–79. doi:10.1016/j.jmps.2017.09.004.

Herring, C., Vogt, E., 1956. Transport and deformation-potential theory for many-valley semiconductors with anisotropic scattering. Physical Review 101, 944–961. doi:10.1103/physrev.101.944.

Imai, T., Uchida, M., Sato, H., Kobayashi, A., 1965. Effect of uniaxial stress on germaniump-nJunctions. Japanese Journal of Applied Physics 4, 102–113. doi:10.1143/jjap.4.102.

Jones, R., Johnson, T., Jordan, W., Wagner, S., Yang, J., Guha, S., 2002. Effects of mechanical strain on the performance of amorphous silicon triple-junction solar cells, in: Conference Record of the Twenty-Ninth IEEE Photovoltaic Specialists Conference, 2002., pp. 1214–1217. doi:10.1109/PVSC.2002.1190826.

Kanda, Y., 1967. Effect of stress on germanium and silicon p-n junctions. Japanese Journal of Applied Physics 6, 475. doi:10.1143/JJAP.6.475.

Kanda, Y., 1991. Piezoresistance effect of silicon. Sensors and Actuators A: Physical 28, 83–91. doi:10.1016/0924-4247(91)85017-i.

Kleimann, P., Semmache, B., Le Berre, M., Barbier, D., 1998. Stress-dependent hole effective masses and piezoresistive properties of p-type monocrystalline and polycrystalline silicon. Phys. Rev. B 57, 8966–8971. doi:10.1103/PhysRevB.57.8966.

Lange, D., Roca i Cabarrocas, P., Triantafyllidis, N., Daineka, D., 2016. Piezoresistivity of thin film semiconductors with application to thin film silicon solar cells. Solar Energy Materials and Solar Cells 145, Part 2, 93–103. doi:10.1016/j.solmat.2015.09.014. selected papers of the EMRS 2015 Spring meeting – Symposium C on Advanced Inorganic Materials and Structures for Photovoltaics.

Nelson, J., 2003. The physics of solar cells. volume 1. Imperial College Press, UK. doi:10.1142/p276.

Pagliaro, M., Ciriminna, R., Palmisano, G., 2008. Flexible solar cells. ChemSusChem 1, 880–891. doi:10.1002/cssc.200800127.

Rindner, W., 1965. Effects of uniaxial and inhomogeneous stress in germanium and silicon p-n junctions. Journal of Applied Physics 36, 2513–2518. doi:10.1063/1.1714521, arXiv:https://doi.org/10.1063/1.1714521.

Rueda, H.A., 1999. Modeling of mechanical stress in silicon isolation technology and its influence on device characteristics. Ph.D. thesis.

Smith, C.S., 1954. Piezoresistance effect in germanium and silicon. Physical Review 94, 42–49. doi:10.1103/physrev.94.42.

Suckow, S., 2014. 2/3-diode fit. URL: https://nanohub.org/resources/14300.

Suckow, S., Pletzer, T.M., Kurz, H., 2012. Fast and reliable calculation of the two-diode model without simplifications. Progress in Photovoltaics: Research and Applications 22, 494–501. doi:10.1002/pip.2301.

Sze, S.M., Ng, K.K., 2006. Physics of semiconductor devices. John wiley & sons. doi:10.1002/0470068329.

Taguchi, M., Maruyama, E., Tanaka, M., 2008. Temperature dependence of amorphous/crystalline silicon heterojunction solar cells. Japanese Journal of Applied Physics 47, 814–818. doi:10.1143/jjap.47.814.

Velut, P., Tween, R., Teuscher, R., Leterrier, Y., Månson, J.A.E., Galliano, F., Fischer, D., 2014. Conformal thin film silicon photovoltaic modules. International Journal of Sustainable Energy 33, 783–796. doi:10.1080/14786451.2013.766611, arXiv:https://doi.org/10.1080/14786451.2013.766611.

Wolf, M., Noel, G., Stirn, R., 1977. Investigation of the double exponential in the current—voltage characteristics of silicon solar cells. IEEE Transactions on Electron Devices 24, 419–428. doi:10.1109/t-ed.1977.18750.

Wooten, F.T., Brooks, A.D., Wortman, J.J., 1968. Effect of uniform stress on si p-n junctions. Proceedings of the IEEE 56, 1221–1222. doi:10.1109/PROC.1968.6527.

Wortman, J.J., Evans, R.A., 1965. Young's modulus, shear modulus, and poisson's ratio in silicon and germanium. Journal of Applied Physics 36, 153. doi:10.1063/1.1713863.

Wortman, J.J., Hauser, J.R., 1966. Effect of mechanical stress on p-n junction device characteristics. ii. generation-recombination current. Journal of Applied Physics 37, 3527–3530. doi:10.1063/1.1708894.

Wortman, J.J., Hauser, J.R., Burger, R.M., 1964. Effect of mechanical stress on p-n junction device characteristics. Journal of Applied Physics 35, 2122–2131. doi:10.1063/1.1702802.